Am J Cancer Res 2026;16(4):1269-1288
www.ajcr.us /ISSN:2156-6976/ajcr0172082

Original Article

Targeting Osteoclastogenesis: Sabutoclax reduces tumor-associated osteolysis and tumor burden within the bone microenvironment

Liang Liao[1,2,3*], Yunde Xu[1,2*], Jindeng Liao[1,2*], Xiaohui Liu[1,2], Jianwen Cheng[1,2,3#], Jinmin Zhao[1,2,3#]

[1]Department of Traumatic Orthopedics and Hand Surgery, The First Affiliated Hospital of Guangxi Medical University, Nanning 530021, Guangxi, China; [2]Guangxi Key Laboratory of Regenerative Medicine, Guangxi Medical University, Nanning 530021, Guangxi, China; [3]Collaborative Innovation Centre of Regenerative Medicine and Medical BioResource Development and Application Co-Constructed by The Province and Ministry, Guangxi Medical University, Nanning 530021, Guangxi, China. [*]Equal contributors. [#]Co-corresponding authors.

Received February 12, 2026; Accepted March 25, 2026; Epub April 15, 2026; Published April 30, 2026

Abstract: Bone metastasis is a major complication of breast cancer, characterized by osteolytic destruction mediated by excessive osteoclast activation. Current anti-resorptive therapies primarily target osteoclasts but have limited impact on the tumor-bone microenvironment vicious cycle that drives bone destruction. This study evaluated the therapeutic efficacy of a novel pan-B-cell lymphoma 2 inhibitor, Sabutoclax, in a breast cancer-induced model osteolysis and explored potential mechanisms associated with its effects. At the cellular level, we assessed the effects of Sabutoclax on the proliferation, invasion, migration, and apoptosis of cancer cells. We observed that Sabutoclax treatment was associated with inhibition of RANKL-induced osteoclast differentiation, RANKL-induced acid secretion, F-actin ring formation, osteoclast bone resorption function, reactive oxygen species (ROS) production, mitogen-activated protein kinase/extracellular signal-regulated kinase signaling, as well as reduced nuclear translocation and expression of nuclear factor of activated T-cells cytoplasmic 1 (NFATc1). In the animal experiment, an orthotopic breast cancer osteolysis model in the tibia of nude mice was established. The in vivo efficacy of Sabutoclax was evaluated. This study found that Sabutoclax effectively prevents breast cancer-induced osteolysis, which may involve a dual mechanism, suppressing breast cancer cell functions and targeting osteoclast differentiation and acid secretion. And the present study only shows that Sabutoclax is associated with ROS reduction, mitochondrial perturbation, and suppression of ERK/NFATc1 signaling. Sabutoclax treatment was associated with both decreased protein expression and reduced nuclear translocation of NFATc1. Future studies could focus on comprehensive evaluation of its pharmacokinetic properties, systemic toxicity, and therapeutic efficacy in more clinically relevant metastatic models to establish its potential application in breast cancer-induced osteolytic bone destruction.

Keywords: Sabutoclax, osteoclast, nuclear factor of activated T-cells cytoplasmic 1, breast cancer

Introduction

Breast cancer shows serious threat to the women's health, often progressing rapidly and frequently accompanied by bone metastasis at advanced stages [1, 2]. According to statistics, about 3% to 10% of women already have metastasis, of which over 70% develop bone metastasis [3]. More than 80% of patients with bone metastasis experience severe bone destruction [4]. The high incidence, elevated metastatic rate, and poor prognosis associated with advanced breast cancer collectively impose greater demands for individualized and precise treatment strategies.

Bone metastasis and bone destruction caused by malignant tumors represent a complex pathological process [5]. Due to the imbalance in the homeostasis between bone formation and resorption, they often manifest as three distinct types, involving osteoblastic, osteolytic, and the mixed. Most bone metastases from breast cancer, however, are characterized by osteolytic destruction [6]. Research indicates that breast cancer bone metastasis results from a

https://doi.org/10.62347/BMGR3542

vicious cycle in the bone microenvironment fueled by tumor cells and osteoclasts. This complex molecular process is regulated by diverse elements such as genetics, transcription factors, signaling pathways, and cytokines [7]. Notably, the bone marrow-derived mononuclear macrophages (BMMs) differentiation into osteoclasts under tumor microenvironment stimulation significantly influences osteolytic severity, yet its precise regulatory mechanisms remain elusive [8, 9]. Consequently, elucidating the molecular mechanisms governing BMM-to-osteoclast differentiation in this context may offer novel perspectives on bone metastasis and destruction, paving the way for targeted therapies for affected patients [10]. Receptor activator of nuclear factor-κB ligand (RANKL), serving as the member of tumor necrosis factor superfamily, effectively promotes osteoclast formation and activation when combined with appropriate concentrations of macrophage colony-stimulating factor (M-CSF) [11, 12]. Furthermore, RANKL also enhances bone resorption by activating relevant signaling pathways that stimulate osteoclast activity [13]. Extensive studies have demonstrated that downstream signaling pathways of RANKL, particularly nuclear factor-κB (NF-κB) and mitogen-activated protein kinase (MAPK), play crucial roles in osteoclast differentiation and functional activation [14]. In breast cancer, aberrant osteoclast differentiation is initiated through both RANKL-dependent pathways [15].

Nuclear factor of activated T cells (NFAT) acts as the transcription factor first identified in activated T cells [16]. Among the family members, nuclear factor of activated T-cells cytoplasmic 1 (NFATc1) resides in the cytoplasm in a highly phosphorylated state under resting conditions [17, 18]. Upon binding of RANK to its ligand RANKL, a cascade of signaling events leads to the NFATc1 nuclear translocation [18]. Once inside the nucleus, NFATc1 directly binds to promoter regions and regulates the expression of characteristic osteoclastogenic target genes, thereby ultimately promoting osteoclast differentiation and function [19]. Studies have shown that NFATc1 knockout mice exhibit severe osteoporosis, and NFATc1 cooperates with FBJ osteosarcoma oncogene (c-Fos) to regulate the process of cell differentiation and maturation [16]. B-cell lymphoma 2 (Bcl-2) contains multiple BH domains [20]. The Bcl-2 gene is highly expressed and positively correlates with tumorigenesis and progression, whereas downregulation or loss of Bcl-2 expression inhibits breast cancer cell growth [21]. The small-molecule compound Sabutoclax is a novel gossypol derivative with pan-BCL-2 inhibitory activity [22]. Sabutoclax binds to BCL-2 and exhibits strong therapeutic efficacy against hematological malignancies [23, 24].

Currently, there is a lack of research on how Sabutoclax affects breast cancer-associated bone destruction and osteolysis. The small-molecule compound Sabutoclax represents a promising targeted therapeutic candidate for inhibiting breast cancer-induced osteolysis. Our experiments demonstrate that Sabutoclax inhibits osteoclast differentiation, RANKL-induced osteoclast differentiation, RANKL-induced acid secretion, formation of the F-actin ring, osteoclast bone resorption function, ROS production, and the mechanism is associated with NFATc1. Furthermore, we are investigating the effects of Sabutoclax of breast cancer-induced tibial osteolysis. This study aims to elucidate the impact of Sabutoclax on breast cancer-driven osteolysis, with the goal of providing a novel therapeutic strategy for treatment.

Materials and methods

Drug

Sabutoclax (Sab, purity ≥99%) was purchased from APExBIO Technology LLC, USA. A 10 mM stock solution of Sabutoclax for osteoclast culture intervention was prepared by dissolving Sabutoclax standard 5 mg in 713.5 μL of dimethyl sulfoxide. RANKL was purchased from R&D Systems, Inc. (USA).

Isolation and culture of mouse BMMs

Euthanize the mouse by rapid cervical dislocation, soak them in 75% alcohol for 5 minutes for disinfection, then remove the soft tissues such as hair and muscle from the bones of the mice's attached lower limbs, and completely extract the bone tissues of the mice's bilateral lower limbs. The bone surfaces were rinsed to remove hair and blood clots, followed by the addition of 10 mL of complete α-minimum essential medium (Thermo Fisher, USA). Residual muscle tissues were further removed from the bones. The bone marrow contents were then flushed out,

and the bones were repeatedly rinsed until the marrow cavities appeared white. The flushed cells were dissociated by pipetting and filtered through a strainer to remove bone fragments and debris. Cell pellet was resuspended and supplemented with an adequate amount of complete α-MEM medium. The medium was replaced once on the day 2.

Cell viability and proliferation assay

Viable cells were measured at indicated time points by cell counting kit-8 (CCK-8) assay (Merck, USA) after the designated period of drug stimulation. Cells were incubated with the specified chemicals of 10 μL CCK8 kit in the dark for 2 hours. The 96-well plate was protected from light and placed in a microplate reader.

Quantitative reverse transcription PCR

To prepare the reverse transcription system, a pre-chilled 1.5 mL Eppendorf tube was placed on ice. 20 μL reaction mixture containing total RNA and RNase-free water was added to the tube. The mixture was gently vortexed, centrifuged at 3000 rpm, and then incubated at 37°C. And the reaction was terminated to inactivate the enzyme. Quantitative reverse transcription PCR was performed using a fluorescent dye-based kit (Thermo Fisher Scientific, USA) to quantify mRNA expression levels.

Western blotting (WB)

Cells were lysed with 150 μL of lysis buffer (Merck, USA), followed by vortexing to fully disrupt the osteoclast proteins. Protein electrophoresis was performed using a vertical electrophoresis system with a 10% separating gel to resolve specific proteins of interest.

A separating gel was prepared and loaded with protein samples alongside a molecular weight marker to identify protein positions. At a constant voltage of 100 V for 90-100 minutes and terminated once the bromophenol blue in the loading buffer migrated to the bottom. Following electrophoresis, proteins were transferred to the nitrocellulose (NC) membrane. After transfer, the membrane was placed in a dark box and blocked.NC membrane was incubated with 10 mL of primary antibody solution, including rabbit anti-mouse IgG such as antibodies against NFATc1, cathepsin K (CTSK), extracellular signal-regulated kinase (ERK), c-Jun N-terminal kinase (JNK), p38 mitogen-activated protein kinase (p38), c-Fos, and β-actin and so on, respectively. The primary antibodies were diluted in blocking buffer as follows: anti-NFATc1 (1:400), anti-CTSK (1:1000), anti-ERK (1:1000), anti-JNK (1:1000), anti-p38 (1:1000), anti-c-Fos (1:500), and anti-β-actin (1:5000). All primary antibodies were purchased from Abcam (USA). Primary antibody incubation was carried out on a shaker at 4°C. Each NC membrane was incubated with secondary antibody goat anti-rabbit IgG solution (1:5000; Abcam, USA), followed by three washes with TBST.

Tumor invasion assay

Upper chamber of the transwell insert was uniformly coated with 100 μL of Matrigel and incubated to allow gel formation. Breast cancer cells were then seeded onto the Matrigel-coated upper chamber, while complete medium containing serum was added to the lower chamber. The plate was placed stained with 0.2% crystal violet (R&D Systems, Inc., USA). Number of invaded tumor cells and the percentage of area covered were quantified.

Wound healing assay

After 48 hours of incubation at room temperature, when the cells reached confluence, a straight scratch was created in each well using a 100 μL pipette tip. The dislodged cells were washed away with PBS (Phosphate-buffered saline). After this period, wound closure was observed using a Leica inverted microscope. The scratch area at each concentration was quantified with ImageJ software.

Flow cytometric analysis

The effect of Sabutoclax on apoptosis in breast cancer cells was investigated. After drug treatment, cell pellets were collected. Following cell counting, the pellets were collected again by centrifugation. For the negative control group, 50 μL of cell suspension was used. For the sample groups, cell suspension was mixed with Annexin V-FITC and propidium iodide (Merck, USA). The mixtures were gently vortexed. Apoptosis was analyzed by flow cytometry within 15 minutes.

Tartrate-resistant acid phosphatase staining and hematoxylin and eosin staining

2,4-Dimethylphenol was dissolved and diluted in 250 mL of ethylene glycol monoethyl ether, followed by the addition of fast garnet GBC salt. A separate solution was prepared by dissolving sodium acetate, sodium tartrate, and acetic acid in ddH_2O. The two solutions were thoroughly mixed to prepare the tartrate-resistant acid phosphatase (TRAP) staining solution (Merck, USA). The cells were fixed with 0.25% formaldehyde solution. The samples were then incubated in a 37°C incubator for approximately 30 minutes and examined under a microscope every 10 minutes until the osteoclasts appeared pink.

The left hind limb of the mouse was dissected and separated, then fixed by immersion in formaldehyde. It was subsequently placed in a decalcification machine for immersion until complete decalcification was achieved. After decalcification of the nude mouse tibia was completed, the tissue samples underwent wax infiltration, embedding, and sectioning. Sections were then subjected to H&E staining and TRAP staining, among other immunohistochemical stains. Finally, imaging and analysis were performed using the BIOQUANTOSTEO fully automated image analysis instrument in the laboratory.

Construction of nude mouse model of breast cancer-induced osteolysis

Twenty-four female nude mice on the C57BL/6 background, aged 6-8 weeks and specific pathogen-free grade, were randomly selected. The mice were housed under standard conditions in an SPF-level animal facility with regular feeding and routine disinfection. All animals survived to the experimental endpoint, with no cases of exclusion. The design and execution of the experiment were approved by the Animal Experiment Committee of Guangxi Medical University, and the experimental procedures complied with the requirements of animal ethics regulations. They were then randomly divided into four groups involving a blank control group, a tumor-positive control group, low-dose and high-dose Sabutoclax treatment group.

The mice were fasted and anesthetized with isoflurane using a small-animal anesthesia machine. The surgical area on the mouse was disinfected with 75% alcohol. A 50 μL suspension containing 1×10^7 MDA-MB-231 cells/mL was drawn up. Using an insulin needle, a minimally invasive puncture was made into the left tibial plateau of the nude mouse, and the cell suspension was injected into the medullary cavity of the tibial plateau. All procedures were performed under strict aseptic conditions. After recovery from anesthesia, returned the mice to their labeled cages and resumed normal feeding. The length, width, and perimeter of the tibial tumor were measured weekly to calculate tumor volume. Sabutoclax was administered every other day. At the end of the experimental period, all mice were humanely euthanized by CO_2 inhalation followed by cervical dislocation.

Micro computed tomography (CT) scanning inspection

Due to the shared nature of the large-scale instrument, limited machine time availability, and the lengthy scanning duration per sample, it was not feasible to complete micro-computed tomography scanning for all 24 specimens within the allocated time slots. Therefore, three mice per group were randomly selected for micro-CT analysis, a sample size consistent with conventional practices in comparable bone microarchitecture studies. No animals were excluded from this experiment. All 24 mice survived to the experimental endpoint, with no cases of unexpected death, infection, or excessive tumor burden requiring exclusion. The remaining mice not subjected to micro-CT analysis were all used for histological analysis, immunohistochemical staining, and molecular biological assays. All data from these analyses have been incorporated into the corresponding sections of the manuscript, with no sample loss due to technical failure. The left tibia of each mouse was harvested and fixed in formaldehyde. Fixed left tibiae of nude mice were then scanned and analyzed using a Micro-CT scanner. Following 3D CT reconstruction of the left tibiae, the extent of tumor-induced bone destruction was analyzed. Quantitative statistical analysis was performed on parameter for each group after drug treatment. Bone samples were scanned using a micro-CT system. For each tibia, a standardized region of interest (ROI) was defined as a 1.0 mm^3 volume located 0.5

mm below the growth plate, extending distally for 2.0 mm. This ROI was consistently applied across all samples to ensure comparability. All micro-CT analyses were performed by an investigator blinded to the experimental groups to minimize bias. The following three-dimensional structural parameters were quantified: bone volume fraction (BV/TV), trabecular number (Tb.N), trabecular thickness (Tb.Th), and trabecular separation (Tb.Sp).

Immunofluorescence assay

Permeabilized with 0.1% Triton X-100, the NFATc1 antibody (Abcam, USA) was diluted and incubated with the cell. The primary antibody solution was collected, and cells were gently washed. Nuclei were stained with DAPI for 5 minutes.

Detection of filamentous actin (F-actin) formation in osteoclasts and ROS

The following day, after cell adhesion, cells in the drug-treated groups were incubated with different concentrations of Sabutoclax (APExBIO Technology LLC, USA). All groups were then cultured continuously for 5 days. On day 6, when mature osteoclasts with large morphology were observed in the RANKL group, the culture medium was completely removed from all wells. The osteoclasts were fixed by incubation with 4% paraformaldehyde in the plates at room temperature for 30 minutes. After one gentle wash with PBS, the cells were permeabilized with 0.1% Triton X-100, followed by blocking. A diluted rhodamine-phalloidin staining solution in 0.2% BSA was added to the plates to stain the F-actin cytoskeleton of osteoclasts, and the plates were incubated for 1 hour. Nuclei were counterstained with DAPI (1:10,000 dilution in PBS). The reactive oxygen species were detected using the Dichlorofluorescein (DCFH) probe.

Measurement of mitochondrial membrane potential

The mitochondrial membrane potential was assessed using the fluorescent probe MitoTracker Red CMXRos (Thermo Fisher Scientific, USA). Briefly, cells were seeded in confocal dishes and treated with indicated concentrations of Sabtouclax (0, 0.2, 0.4 μM) in the presence of RANKL for the designated time. After treatment, cells were incubated with 200 nM MitoTracker Red CMXRos in pre-warmed culture medium at 37°C for 30 min in the dark. Following incubation, cells were gently washed twice with pre-warmed PBS to remove excess probe. Fluorescence images were immediately acquired using a confocal laser scanning microscope (Zeiss LSM 880) with excitation at 579 nm and emission collected at 599 nm. All imaging parameters involving laser power and gain, pinhole were kept constant across all experimental groups to ensure comparability.

Bone acid secretion assay by osteoclasts

BMMs were seeded into confocal-compatible culture dishes. The following day, after stable cell adhesion, the drug-treated groups were incubated with different concentrations of Sabutoclax. Following three rounds of drug administration, mature osteoclasts appeared in the positive control wells. The cells were then washed three times with PBS. An acidic fluorescent dye, acridine orange, was added, and the dishes were returned to the 37°C incubator for an additional 30 minutes of incubation. After three subsequent washes with PBS, images were captured under a fluorescence microscope and subjected to statistical analysis.

Statistical analysis

Statistical analysis was conducted using SPSS 19.0 (IBM, California, USA), and graphs were generated ultilizing GraphPad Prism 8.0 (California, USA). Normality tests were conducted. Data analyzed by one-way ANOVA are expressed as mean ± standard deviation. Statistical analysis was performed using one-way ANOVA with Tukey's post hoc test. The $P<0.05$ was considered statistically significant.

Results

Inhibition by Sabutoclax of RANKL-induced osteoclast differentiation and RANKL-induced acid secretion

To determine whether Sabutoclax exerts toxic effects on osteoclast precursor cells, we assessed its cytotoxicity against BMMs using the CCK-8 assay after 48 hours of drug intervention with various concentrations (0, 0.1, 0.2, 0.3, 0.4, 0.5, 0.6, 0.7, 0.8, 0.9, and 1.0 μM). The results (**Figure 1A**) show the molecular str-

ucture of Sabutoclax. Treatment with Sabutoclax for 48 hours at concentrations ≤0.5 μM showed no cytotoxicity toward BMMs (**Figure 1B**). The IC_{50} of Sabutoclax was calculated to be 0.89 μM (**Figure 1C**). This experiment evaluated the impact of different concentrations of Sabutoclax on the viability of BMMs during culture. The CCK-8 assay results indicated no significant statistical difference in absorbance between the Sabutoclax groups and the control group (P>0.05), demonstrating that Sabutoclax at 0.1-0.5 μM exerts no toxic effect on BMMs.

We investigated how Sabutoclax affects osteoclast differentiation. Osteoclast differentiation was induced by treating BMMs with RANKL, followed by intervention with Sabutoclax at concentrations of 0.1, 0.2, 0.3, and 0.4 μM. The results (**Figure 1D**) show that Sabutoclax at a concentration of 0.2 μM significantly inhibited osteoclast differentiation, and this effect was concentration-dependent.

Additionally, statistical analysis of osteoclast numbers in each group revealed that Sabutoclax at 0.1 μM (P<0.05), 0.2 μM (P<0.01), 0.3 μM (P<0.001), and 0.4 μM (P<0.001) significantly inhibited osteoclast fusion and formation compared to the positive control group (**Figure 1E**). Therefore, we conclude that Sabutoclax can inhibit osteoclast differentiation and formation. Compared to the positive control, treatment with 0.2 μM Sabutoclax reduced the number of osteoclasts by more than 50%, and the cell morphology appeared notably smaller. At a concentration of 0.3 μM, the reduction in cell number exceeded 80%, and the cell volume was also significantly suppressed. At a concentration of 0.4 μM, the formation of mature osteoclasts was almost completely inhibited.

To further understand the effect of Sabutoclax on the secretory function of osteoclasts, we experimentally validated the impact of Sabutoclax on bone resorption function. Using fluorescence-based assays to study acid secretion in osteoclasts, we found that Sabutoclax inhibits the acid-secreting capacity of osteoclasts (**Figure 1F**). A statistically significant difference was observed between the Sabutoclax-treated group and the RANKL-induced positive control group (**Figure 1G**).

Inhibition by Sabutoclax of formation of the F-actin ring in osteoclasts and ROS production

The study investigated the effect of different concentrations of Sabutoclax on the formation of F-actin rings in osteoclasts. As shown in **Figure 2A**, after the addition of Sabutoclax, the formation of F-actin rings significantly decreased, and this effect was concentration-dependent. Additionally, through statistical analysis, Sabutoclax at 0.2 μM and 0.4 μM (P<0.001) could significantly inhibit the F-actin rings in osteoclasts, and the difference was statistically significant (**Figure 2B**, **2C**). Sabutoclax can also inhibit the production of ROS and mitochondrial membrane potential in osteoclasts at concentrations of 0.2 μM and 0.4 μM (**Figure 2D**, **2E**).

Inhibition by Sabutoclax of osteoclast bone resorption function induced by RANKL

After the intervention with Sabutoclax, the area of the bone slice's absorption pit surface became smaller and shallower, and the osteoclast's bone absorption activity was inhibited (**Figure 3A**). Sabutoclax at concentrations of 0.2 μM and 0.4 μM (P<0.001) was able to significantly reduce the area of bone resorption pits in osteoclasts, and the difference was statistically significant (**Figure 3B**). Statistical analysis showed that the number of TRAP staining in osteoclasts was reduced. Sabutoclax was able to inhibit the bone resorption function of mature osteoclasts (**Figure 3C**, **3D**).

Inhibition of mature osteoclastic acid secretory and bone resorption function by Sabutoclax

In the present study, Sabutoclax was administered throughout the osteoclast differentiation period. The experimental design clearly demonstrates the inhibitory effect of Sabutoclax on RANKL-induced osteoclast differentiation. After the formation of mature osteoclasts, we added Sabutoclax and then conducted functional tests. We found that the mature osteoclast acid secretion and bone resorption functions were inhibited by Sabutoclax (**Figure 4A**, **4B**).

Inhibition of MAPK/ERK signaling in osteoclasts, the nuclear translocation, and expression of NFATc1 by Sabutoclax treatment

As shown in **Figure 5A** and **5B**, phosphorylation of ERK peaked at the 10-minute time point. In the presence of Sabutoclax, Sabutoclax can inhibit ERK protein phosphorylation. **Figure 5C**,

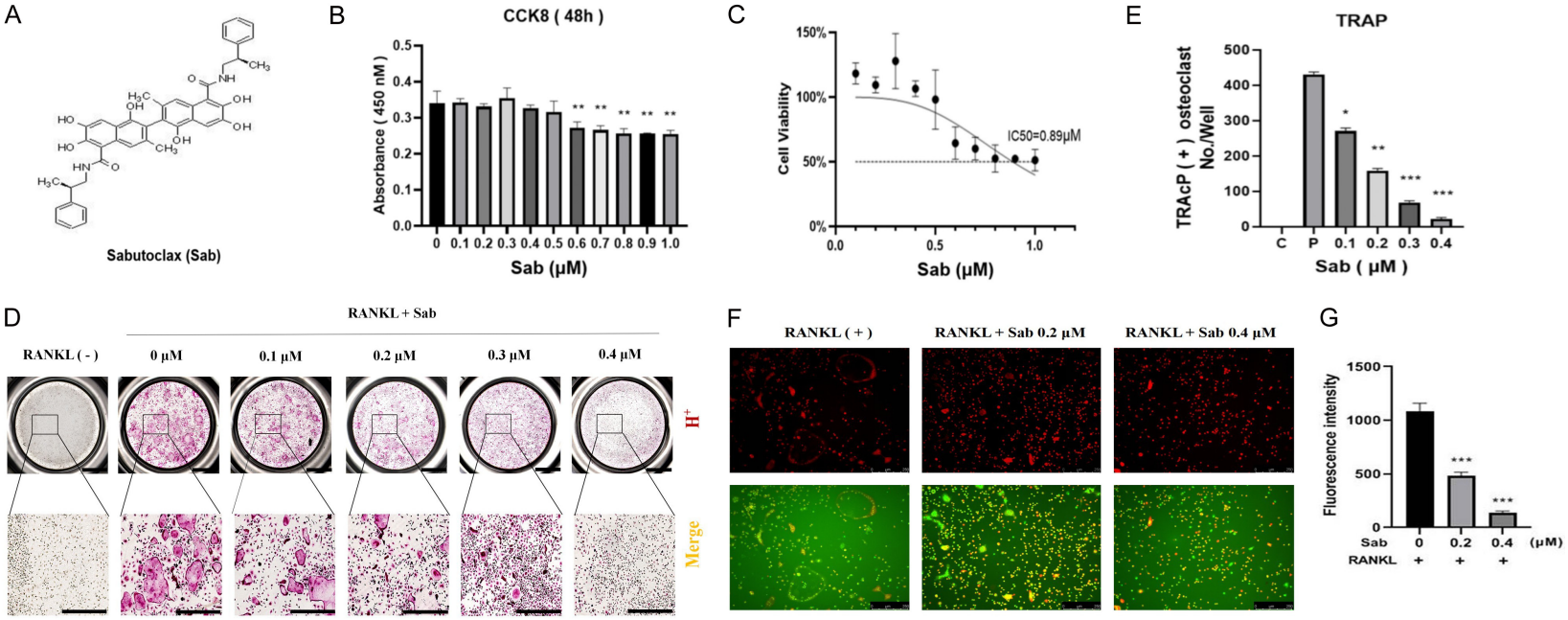

Figure 1. Sabutoclax inhibitsRANKL-induced osteoclast differentiation and RANKL-induced acid secretion. A. Diagram of the chemical structure of Sabutoclax. B. Statistical analysis of the absorbance of Sabutoclax on a BMMs microplate reader at 450 nm. C. Cell viability results with Sabutoclax in BMMs IC50 value line 0.89 μM (N=3). D. TRAP staining plots for the drug concentration dependent inhibition of osteoclast fusion and generation by Sabutoclax. N=3, scale bar = 1000 μm. E. Statistical analysis graphical representation of Sabutoclax drug concentrations per group corresponding to the number of cells in culture wells that stained positive for osteoclast fusion and generated TRAP and had ≥3 nuclei. F. Fluorescence microscope photograph found that sabutoclax could inhibit osteoclastic acid secretory function. Scale bar = 100 μm, N=3. G. After sabutoclax treatment, the fluorescence intensity of secreted acid from osteoclasts in each group was quantified by statistical analysis. $^{*}P<0.05$, $^{**}P<0.01$, $^{***}P<0.001$. RANKL, receptor activator of nuclear factor-κB ligand; BMMs, bone marrow-derived macrophages; TRAP, tartrate-resistant acid phosphatase.

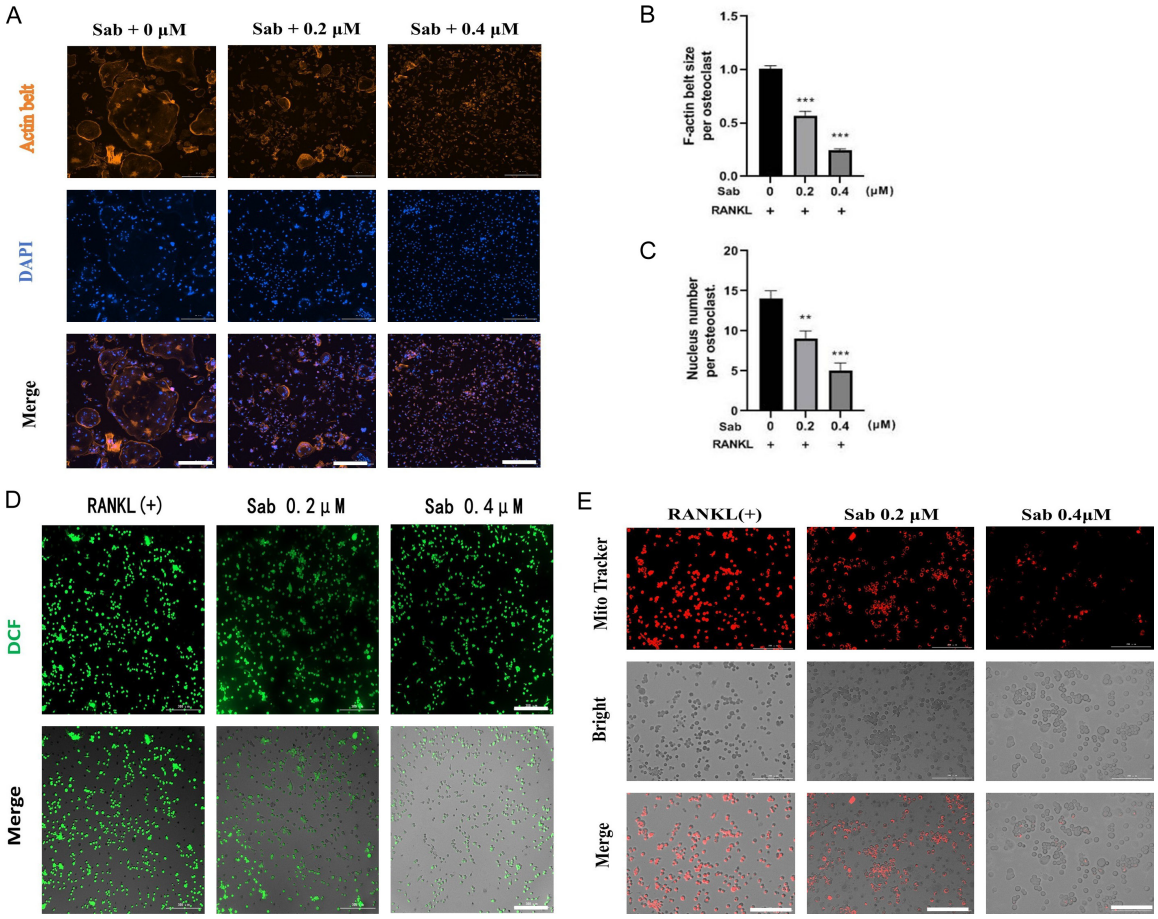

Figure 2. Sabutoclax inhibits formation of the F-actin ring in osteoclasts and ROS production. A. Immunofluorescence staining was used to detect the formation of F-actin, a fibrin ring of osteoclasts. N=3, scale bar = 1000 μm. B, C. Statistical analysis F-actin size quantification in each field and the number of nuclei within each osteoclast. D. 2',7'-Dichlorofluorescein (DCF) results of ROS production. N=3, scale bar = 300 μm. E. Effects of Sab on mitochondrial membrane potential in RANKL-stimulated cells. N=3, scale bar = 200 μm. $^{*}P<0.05$, $^{**}P<0.01$, $^{***}P<0.001$. ROS, reactive oxygen species; DCF, 2',7'-Dichlorofluorescein.

5D show that after intervention with 0.4 μM Sabutoclax, quantitative analysis of the gray-scale values for p-JNK/JNK and p-P38/P38 revealed no statistically significant differences.

The differentiation and maturation of osteoclasts depend on the sustained expression and activation of proteins such as c-Fos, CTSK, and NFATc1. We examined the effect of Sabutoclax on the expression of these proteins by Western blotting. The results (**Figure 5E**) showed that, following treatment with Sabutoclax, the expression levels on days 1, 3, and 5 were all reduced compared to the RANKL-only control group. As quantified by ImageJ software (**Figure 5F-H**), the RANKL-induced increases in the grayscale ratios of c-Fos and NFATc1 to their loading controls on days 3 and 5, respectively, were significantly attenuated by Sabutoclax treatment. Furthermore, Sabutoclax intervention also led to a statistically significant suppression in the expression levels of NFATc1 and CTSK on both day 3 and day 5.

NFATc1 drives the expression of osteoclast-specific genes, thereby promoting cell fusion and bone resorption. Immunofluorescence analysis revealed that Sabutoclax inhibited the nuclear translocation of NFATc1 in BMMs (**Figure 5I**). In Sabutoclax-treated cells, the NFATc1 signal (green) was largely excluded from DAPI-stained nuclei, whereas RANKL stimulation led to clear nuclear co-localization. Consistently, a dual-luciferase reporter assay confirmed that Sabutoclax suppressed NFATc1 transcriptional activity (**Figure 5J**).

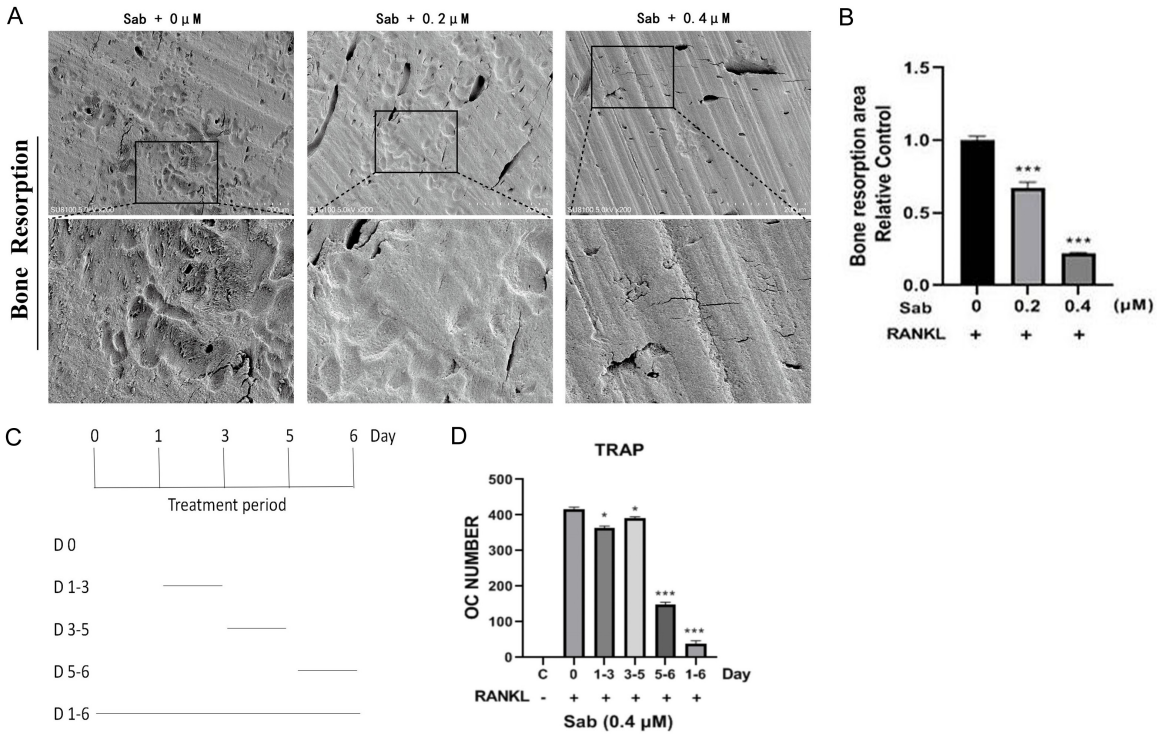

Figure 3. Sabutoclax inhibits osteoclast bone resorption function induced by RANKL. A. Sabutoclax inhibits bone resorption area of mature osteoclasts in bone slices. B. Statistical analysis quantified values of osteoclastic bone resorption area on bovine bone slices in each group. C. Schematic diagram of the administration period. D. Statistical analysis corresponds to the number of osteoclast trap staining. N=3, scale bar = 200 μm, $^{*}P<0.05$, $^{***}P<0.001$. RANKL, receptor activator of nuclear factor-κB ligand.

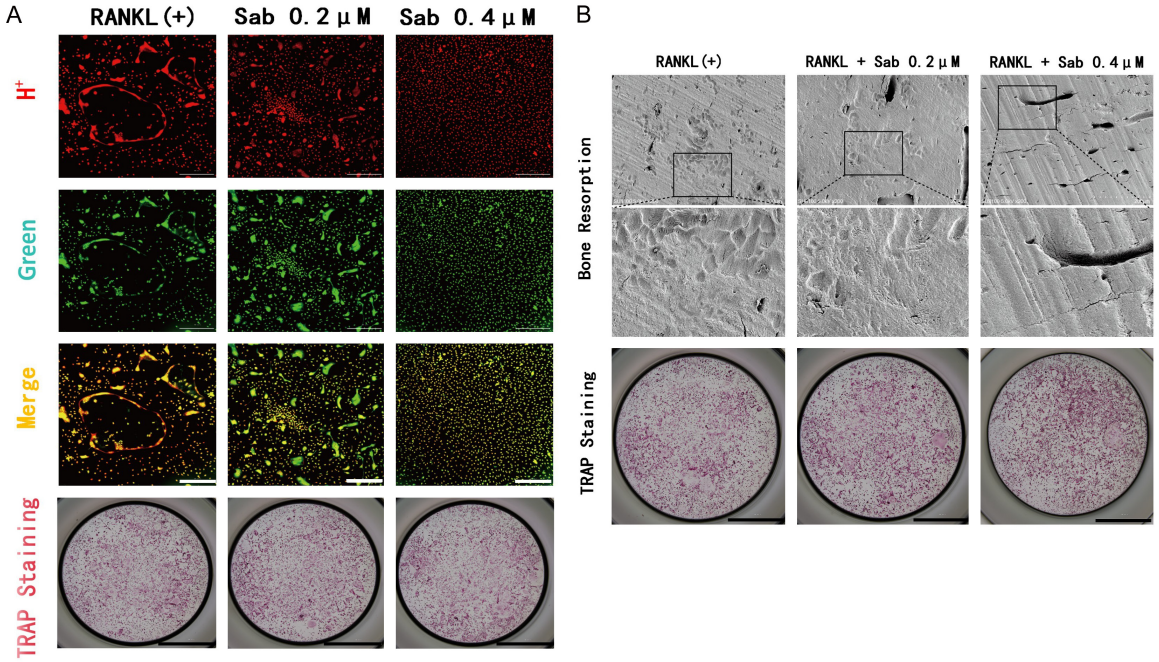

Figure 4. Sabutoclax inhibit mature osteoclastic acid secretory and bone resorption function. A. Fluorescence microscope photograph found that sabutoclax could inhibit mature osteoclastic acid secretory function. Scale bar = 100 μm in the fluorescence image, N=3. B. Sabutoclax can inhibit the bone resorption function of mature osteoclasts. N=3, scale bar = 200 μm.

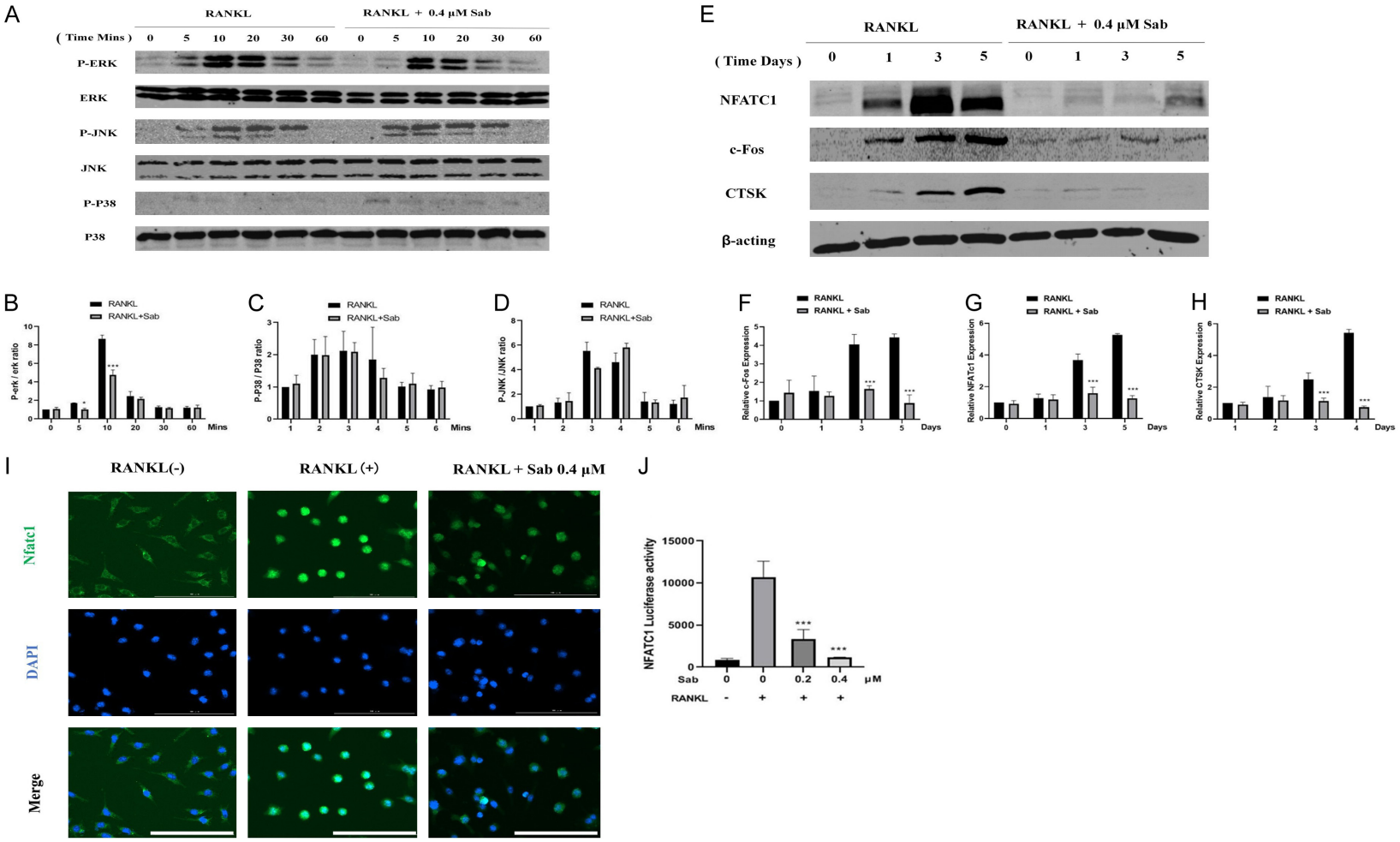

Figure 5. Sabutoclax inhibits MAPK/ERK signaling in osteoclasts and the nuclear translocation and expression of NFATc1 (N=3). A. Sabutoclax inhibits phosphorylation of ERK protein expression. B-D. The ratios of phosphorylated to total proteins of ERK, JNK, and p38 in each group were statistically analyzed. E. Sabutoclax inhibits c-Fos, CTSK, and NFATc1 protein expression (N=3). F-H. Statistical analysis of the ratios of c-Fos, CTSK, and NFATc1 proteins to the corresponding β-actin. I, J. Immunofluorescence plots show that Sabutoclax inhibits RANKL induced nuclear translocation of NFATc1 in osteoclasts. Luciferase reporter assays showed that Sabutoclax intervention treatment was able to inhibit RANKL induced transcriptional activity of the NFATc1 gene. The resulting data were used as described by the mean ± standard deviation. N=3, scale bar = 1000 μm in the figure, $^{*}P<0.05$, $^{**}P<0.01$, $^{***}P<0.001$. MAPK/ERK, mitogen-activated protein kinase/extracellular signal-regulated kinase; NFATc1, nuclear factor of activated T-cells cytoplasmic 1; JNK, c-Jun N-terminal kinase; p38, p38 mitogen-activated protein kinase; c-Fos, FBJ osteosarcoma oncogene; CTSK, Cathepsin K.

These observations suggest a potential correlation between Sabutoclax treatment and selective inhibition of the ERK pathway, whether this reflects a direct causal relationship requires further investigation.

Inhibition of proliferation, migration, and invasion in breast cancer by Sabutoclax

The effect of Sabutoclax on breast cancer cell migration was confirmed by a scratch assay. We found that Sabutoclax inhibited the wound healing of MDA-MB-231 cells. In the assay, cells were treated with 0.2, 0.4, 0.8, and 1.6 μM Sabutoclax, and wound closure was compared at 0 and 24 hours. The wound healing percentage decreased from 31.30% ± 1.78% in the untreated group to 24.86% ± 2.71%, 20.08% ± 1.53%, 21.75% ± 2.63%, and 18.87% ± 3.98%, respectively. These results indicate that Sabutoclax inhibits the horizontal migration (**Figure 6A**).

Furthermore, we used a transwell assay to evaluate the inhibitory effect of Sabutoclax on the invasion. In this assay, cells were treated with Sabutoclax for 24 h, after which the lower chamber membrane was fixed, stained, photographed under a microscope, and statistically analyzed to count the invaded cell number. We observed a reduction in the number of invading cells after 24 h of Sabutoclax treatment compared to the control group, and the differences compared to the 0 μM (no drug) group were statistically significant (**Figure 6B-D**).

Induction of apoptosis and gene expression in breast cancer cells by Sabutoclax

Apoptosis in MDA-MB-231 cells treated with Sabutoclax was assessed by flow cytometry. The proportion of apoptotic cells was significantly increased in the Sabutoclax-treated groups, with a more pronounced increase in early apoptosis. The early apoptotic rate rose from 0.73% in the blank control to 2.09%, 2.41%, 2.94%, and 4.9% after treatment with 0, 0.2, 0.4, 0.8, and 1.6 μM Sabutoclax, respectively. The total apoptotic cell ratio also increased, from 1.74% in the blank control to 2.4%, 2.78%, 3.28%, and 4.9% after treatment with 0.2, 0.4, 0.8, and 1.6 μM Sabutoclax, respectively. These results confirm that Sabutoclax promotes apoptosis in MDA-MB-231 cells (**Figure 7A-C**).

PCR results indicated that treatment with different concentrations of Sabutoclax for 48 hours increased the expression of BAX but downregulated the expression of BCL-2 (**Figure 7D**, **7E**). These observations demonstrate that Sabutoclax treatment correlates with an elevated apoptotic rate in MDA-MB-231 cells, concurrent with upregulated BAX expression and downregulated BCL-2 expression, implicating the potential engagement of the mitochondrial apoptotic pathway.

Treatment of osteolytic bone lesions with Sabutoclax

We further investigated the therapeutic effect of Sabutoclax on breast cancer-induced osteolytic lesions. Compared to the PBS-treated control group, treatment with Sabutoclax significantly reduced tumor size and volume (**Figure 8A-C**). In vivo imaging revealed high-intensity luminescence signals in the lower limbs of tumor-bearing mice in the positive control group, whereas the signal intensity in the Sabutoclax-treated groups was attenuated (**Figure 8D**).

Sabutoclax inhibiting tumor growth of tumor burden within the bone microenvironment in vivo

Micro-CT imaging revealed that mice in the tumor-positive control group exhibited severe osteolytic bone loss. Treatment with Sabutoclax provided protection against bone destruction in the model (**Figure 9A**). Micro-CT analysis showed in **Figure 9B-E**. These results indicate that Sabutoclax treatment can protect against and mitigate tumor burden within the bone microenvironment-induced osteolysis and bone damage.

Extensive trabecular bone loss in the tumor-bearing tibiae of the positive control group. Sabutoclax-treated group exhibited a significant reduction in TRAP-positive osteoclasts on the bone surface (**Figure 9F**). Therefore, these results indicate that Sabutoclax can alleviate breast cancer metastasis-induced osteolytic lesions by inhibiting osteoclastogenesis and bone resorption. In conclusion, Sabutoclax protects against breast cancer-induced tibial bone loss *in vivo*.

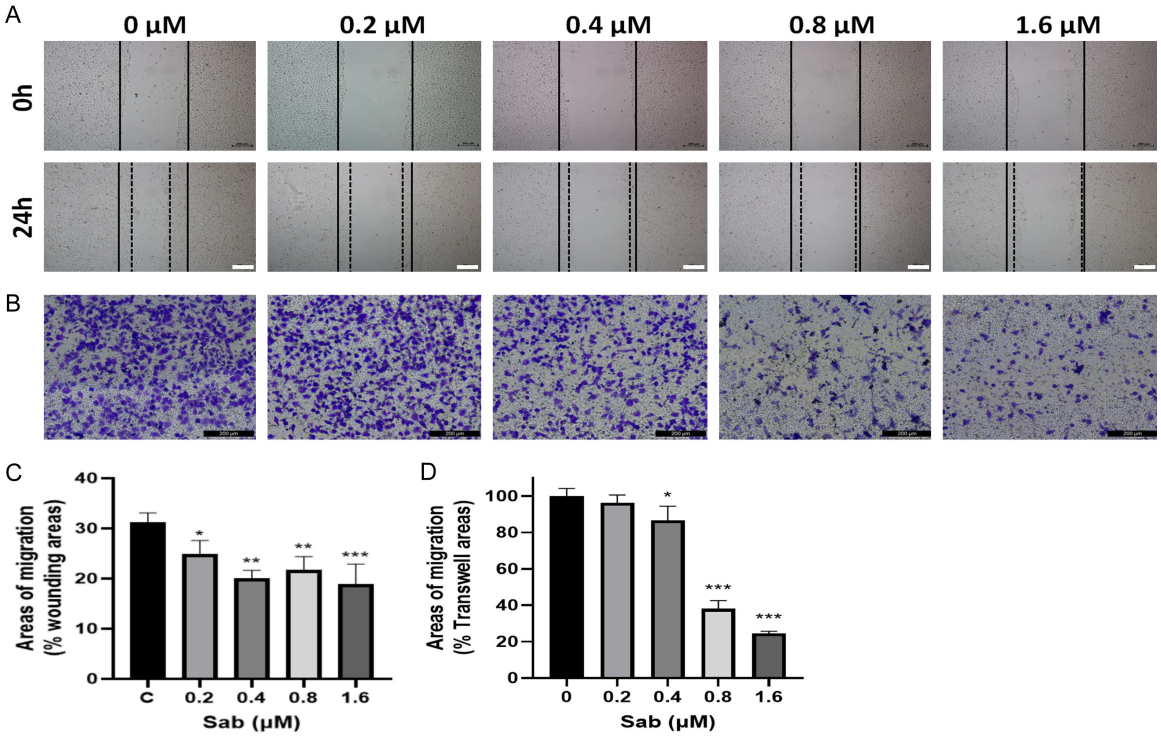

Figure 6. Sabutoclax inhibits the proliferation, migration, and invasion of breast cancer MDA-MB-231 cells. A. The area of scratch area after 0 h and 24 h of Sabutoclax effect, it can be seen that Sabutoclax inhibited the migration of MDA-MB-231 cells compared with the control group. B. Sabutoclax reduces the number of cells invaded by MDA-MB-231 cells showed that Sabutoclax inhibited the invasion of MDA-MB-231 cells. C, D. Statistical analysis of the wound healing area of cells and the number of invasion, mean ± standard deviation. N=3, scale bar = 200 μm, $^{*}P<0.05$, $^{**}P<0.01$, $^{***}P<0.001$.

Discussion

Complications arising from bone metastasis in advanced breast cancer, including osteolysis and bone destruction, significantly compromise patient quality of life [25]. Breast cancer incidence reached 2.26 million, surpassing lung cancer to become the leading cancer globally [25]. Bone homeostasis relies on a dynamic balance between the functions of osteoblasts and osteoclasts [26]. Bone metastasis is the most common form of terminal breast cancer dissemination, frequently occurring in the spine, long bones, and pelvis [27]. Resident osteoclasts within the bone are activated by cytokines such as IL-1, IL-6, and TNF-secreted by bone-metastatic breast cancer cells. In turn, these activated osteoclasts secrete tumor growth factors, further fueling a vicious cycle that stimulates tumor growth, accompanied by bone structural destruction and osteolysis [28]. Previous research has demonstrated that Sabutoclax, a pan-Bcl-2 inhibitor, effectively suppresses the growth of cell lines derived from various human cancers, including prostate, ovarian, lung, colorectal cancers, and lymphoma [29, 30]. However, the impact of Sabutoclax on tumor-associated osteolysis and tumor burden within the bone microenvironment has not yet been documented.

Osteoclasts originate from monocyte/macrophage progenitors of human myeloid hematopoietic stem cells. Under induction by various cytokines, monocytic precursor cells undergo a series of steps including intercellular fusion, formation, and maturation, ultimately fusing into multinucleated giant cells known as osteoclasts. Currently, numerous studies have demonstrated that Sabutoclax possesses pharmacological effects such as antioxidant and anti-tumor activities. However, its role in skeletal system diseases, particularly its effect on osteoclasts, has not been reported. In this study, we first screened safe concentrations of Sabutoclax using the CCK-8 cell proliferation assay for subsequent experiments. Subsequently, employing an in vitro RANKL-induced

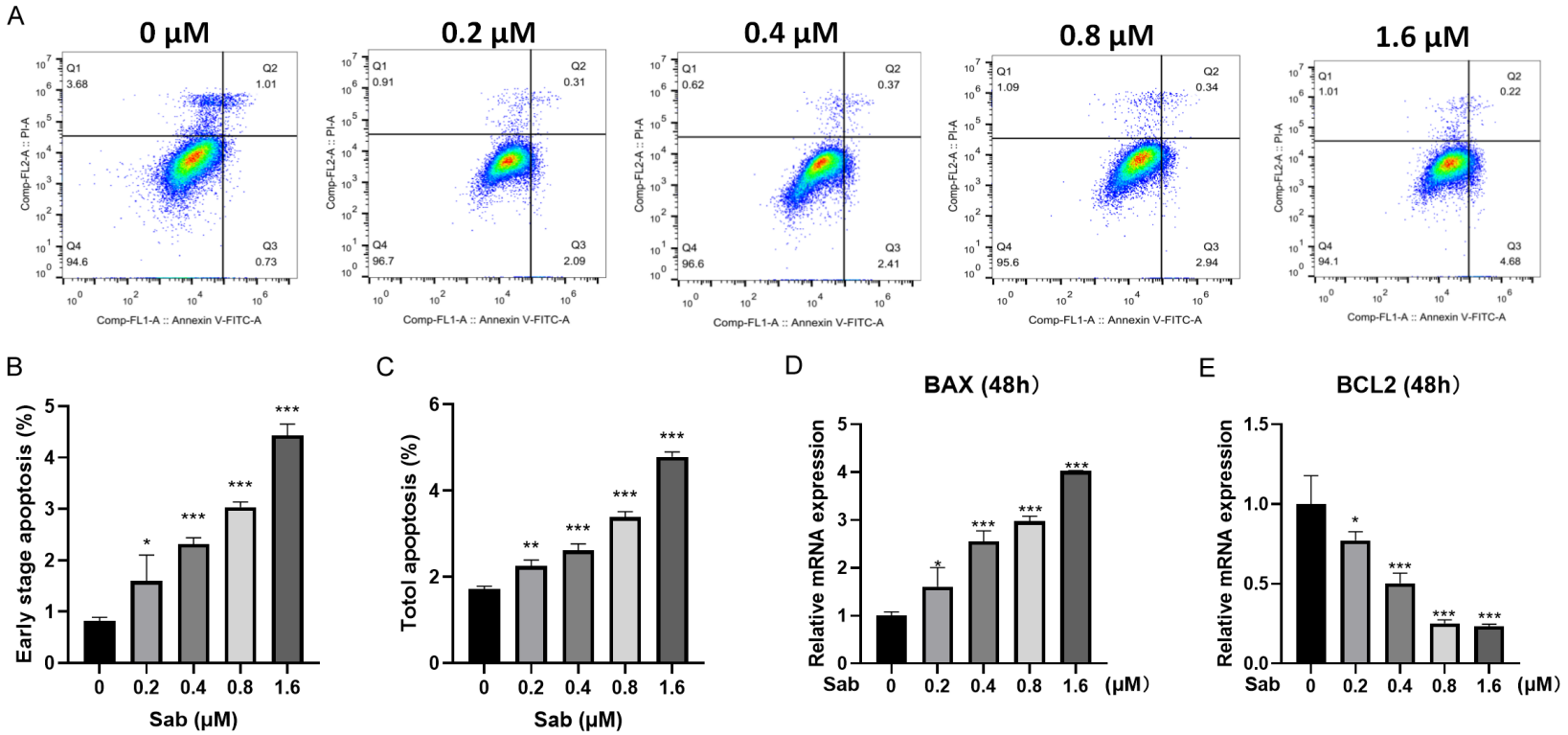

Figure 7. Sabutoclax induces apoptosis and gene expression in MDA-MB-231 breast cancer cells. A. Flow cytometric plots of each concentration group, promoting cell early apoptosis versus late apoptosis. B, C. Statistical results obtained after analysis: early apoptosis from 0.73% of the blank control group, to 0 μM, 0.2 μM, 0.4 μM, 0.8 μM, and 1.6 μM Sabutoclax post intervention increased to 2.09%, 2.41%, 2.94%, 4.9% vs. % of the total apoptotic cell ratio, 1.74% of the blank control to 0.2 μM, 0.4 μM, 0.8 μM, and 1.6 μM Sabutoclax and then increased to 2.4%, 2.78%, 3.28%, 4.9%, respectively. D, E. The results showed that different concentrations of 0.2 μM, 0.4 μM, 0.8 μM, and 1.6 μM elevated expression of Bax and downregulated expression of Bcl-2 at 48 h after Sabutoclax treatment. Statistical analysis of the wound healing area of cells and the number of invasion, mean ± standard deviation (N=3, $^{*}P<0.05$, $^{**}P<0.01$, $^{***}P<0.001$).

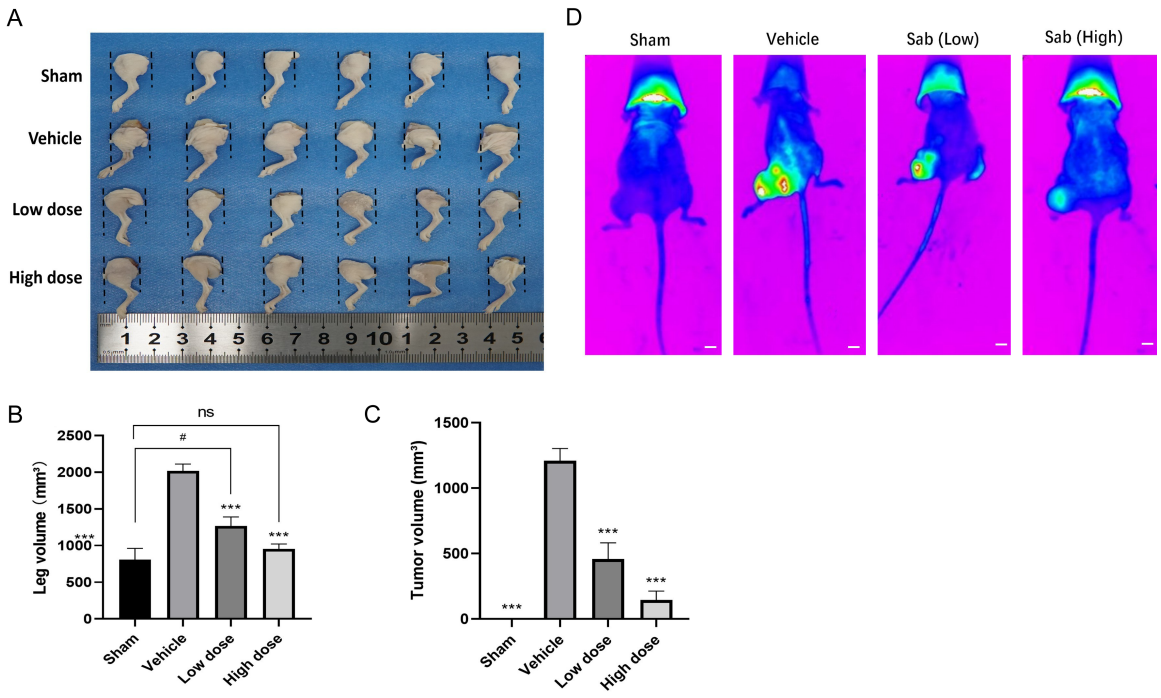

Figure 8. Sabutoclax functioned to inhibit the tumor growth of tumor burden within the bone microenvironment in vivo. A. The view of the left lower extremity of each group of mice. B, C. The mean and standard deviation of tumor length and width of individual mice in each group were measured using vernier calipers. D. *In vivo* imaging confirmed that the inhibitor Sabutoclax effectively suppresses tumor growth of breast cancer bone metastases. Statistical analysis of the wound healing area of cells and the number of invasion, mean ± standard deviation (N=3, scale bar = 10 cm, $^{\#}P<0.05$, $^{*}P<0.05$, $^{**}P<0.01$, $^{***}P<0.001$).

osteoclast fusion and formation model, we confirmed through CCK-8 assays and TRAP staining that Sabutoclax, within a safe concentration range, can inhibit RANKL-induced osteoclast fusion and formation. Besides, Sabutoclax treatment was associated with reduced protein expression of c-Fos, CTSK, and NFATc1.The activation of NFATc1 drives its own expression through an auto-amplification mechanism [31]. Sabutoclax treatment was associated with both decreased protein expression and reduced nuclear translocation of NFATc1. The transcription factor NFATc1 plays a pivotal role in the fusion and formation of osteoclasts, and is essential for their proliferation, fusion, formation, adhesion, and bone-resorptive functions [32]. Following the binding of RANK to its ligand RANKL, a cascade of signaling events leads to the nuclear translocation of NFATc1 [33]. Once inside the nucleus, NFATc1 directly binds to promoter regions. Sabutoclax treatment was associated with downregulation of key osteoclast-related genes, which may contribute to reduced osteoclast proliferation, fusion, and maturation [34]. The MAPK pathway signaling cascade, comprising the sequential activation of MAPKKK, MAPKK, and MAPK, regulates osteoclastogenesis through phosphorylation-driven control of gene expression, cell fate, and differentiation. Our current data indicate that Sabutoclax treatment is associated with reduced ERK phosphorylation, decreased NFATc1 expression/nuclear translocation, and impaired osteoclast differentiation, but cannot prove a causal relationship among these events. We have established a phenotypic link between pan-BCL-2 inhibition and impaired osteoclastogenesis; however, the proposed ERK-NFATc1 signaling axis is based on correlative observations and remains speculative rather than a validated causal mechanism. As a pan-BCL-2 inhibitor, Sabutoclax is expected to primarily target BCL-2 family proteins. In the present study, we did not examine the expression levels of BCL-2, BCL-XL, or MCL-1 in osteoclast precursor cells. Therefore, whether Sabutoclax exerts its effects through its canonical mitochondrial targets in this context remains to be confirmed. Furthermore, while our data suggest that Sabutoclax treatment is associated with reduced

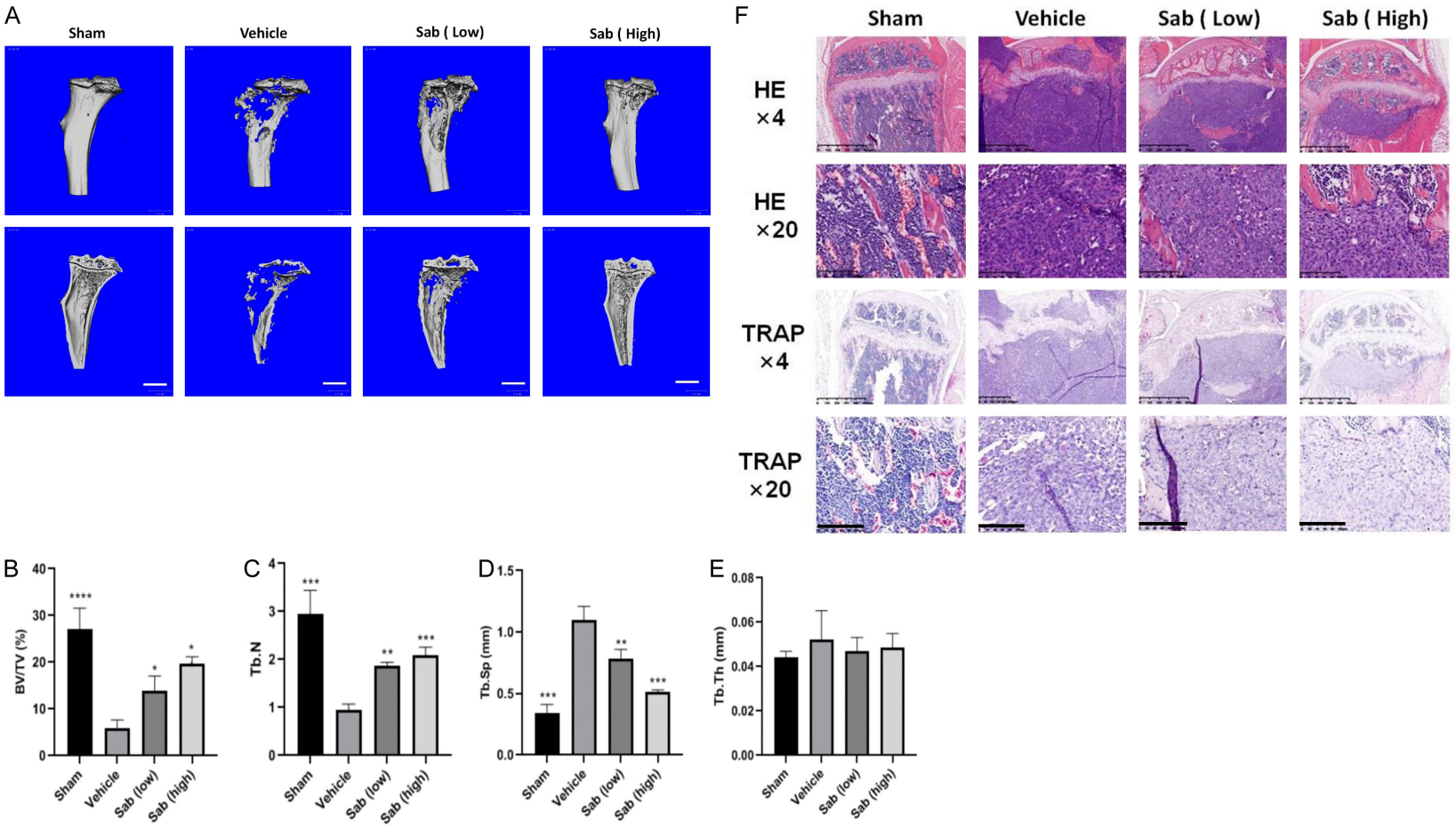

Figure 9. Sabutoclax inhibits breast cancer bone induced osteolysis and osteolytic trabecular bone loss in mice. A. Micro-CT results showed that tumor-associated osteolysis could be compared positive with negative control group to induce the occurrence of severe osteolysis, high concentration group, compared with low concentration group, could find remission of bone destruction situation (N=3, scale bar =1.0 mm). B-E. The CT quantification analysis was performed for each group, measuring parameters including BV, BS, TV, Tb.Sp, Tb.N, and Tb.Th. The statistical results demonstrated that Sabutoclax alleviates bone destruction within the bone microenvironment. F. Histomorphometric H&E staining confirmed that Sabutoclax inhibited osteolytic trabecular bone loss in tibiae of mice with breast cancer osteoinduction. Trap staining results showed that the number of osteoclasts decreased in the drug treated group, and especially, a significant decrease in trap positive osteoclasts on the trabecular bone surface could be observed after treatment with a high concentration of Sabutoclax (N=3, scale bar = 100 μm). Statistical analysis of the wound healing area of cells and the number of invasion, mean ± standard deviation. $^{*}P<0.05$, $^{**}P<0.01$, $^{***}P<0.001$. H&E staining, hematoxylin and eosin staining; Micro-CT, Micro-computed tomography; BV, bone volume; BS, bone surface; TV, tissue volume; Tb.Sp, trabecular separation; Tb.N, trabecular number; Tb.Th, trabecular thickness.

ERK phosphorylation and impaired NFATc1 nuclear translocation, these findings remain correlative. We did not perform functional gain- or loss-of-function experiments such as BCL-2 knockdown to mimic Sabutoclax effects, or BCL-2 overexpression to rescue NFATc1 inhibition which would be necessary to establish a causal role for BCL-2. Similarly, rescue experiments using ERK activators such as TPA treatment and constitutively active ERK constructs are required to determine whether ERK inhibition is mechanistically upstream of NFATc1 suppression. Without such experiments, the proposed ERK-NFATc1 axis represents a pathway association rather than a closed mechanistic loop. In summary, our findings indicate that Sabutoclax treatment correlates with inhibition of ERK phosphorylation, reduced NFATc1 expression/nuclear translocation, and impaired osteoclast differentiation. However, the precise molecular mechanisms particularly the causal relationships among BCL-2 inhibition, ERK signaling, and NFATc1 regulation require further investigation through genetic and pharmacological rescue experiments.

Sabutoclax inhibits ROS production and impacts mitochondrial membrane potential in RANKL-stimulated cells. The current study should be viewed as a preliminary observation that establishes a phenotypic link between pan-BCL2 inhibition and osteoclastogenesis, rather than a definitive mechanistic dissection. We acknowledge that the precise molecular mechanisms, particularly regarding ROS source specificity and calcium signaling, remain speculative and require further investigation. Based on the established role of BCL-2 family proteins in regulating mitochondrial permeability and endoplasmic reticulum (ER) calcium homeostasis, we speculate on several possible mechanisms by which Sabutoclax may inhibit RANKL-induced osteoclastogenesis, although these hypotheses require direct experimental validation. First, given that RANKL-induced ROS production derived from both mitochondrial respiration and NADPH oxidase (Nox1/2) activity serves as a critical signal for NFATc1 activation [31]. It is plausible that Sabutoclax disrupts ROS signaling. Our data show that Sabutoclax reduces total intracellular ROS levels (as measured by DCFH staining). However, this assay does not distinguish between mitochondrial ROS and Nox-derived ROS. Therefore, whether Sabutoclax primarily affects mitochondrial ROS leakage, inhibits Nox enzyme activity, or both, remains to be determined. Future studies using MitoSOX staining (for mitochondrial superoxide) and selective Nox inhibitors would clarify the specific source of ROS affected by Sabutoclax. Second, BCL-2 localized to the ER membrane plays a well-characterized role in buffering ER calcium release [11]. RANKL stimulation induces sustained low-frequency calcium oscillations, which are essential for maintaining calcineurin-mediated NFATc1 dephosphorylation and nuclear retention. Inhibition of BCL-2 by Sabutoclax could theoretically alter ER calcium handling, potentially disrupting these oscillations. However, in the present study, we did not directly assess calcium flux, calcineurin activity, or NFATc1 phosphorylation status. Consequently, whether Sabutoclax affects the calcium-calcineurin-NFATc1 axis remains an open question.In summary, while our data clearly demonstrate that Sabutoclax inhibits osteoclast differentiation and reduces total ROS levels, the precise molecular mechanisms particularly regarding ROS sources and calcium signaling require further investigation. Studies employing live-cell calcium imaging, phospho-specific antibodies for MAPKs and NFATc1, and genetic or pharmacological dissection of ROS sources will be necessary to definitively establish the mechanisms proposed here.

We confirmed the in vivo efficacy of Sabutoclax in inhibiting bone destruction and preserving bone structure. Cellular studies further revealed that Sabutoclax curbs MDA-MB-231 cell proliferation, migration, and invasion, and induces apoptosis in vitro. These combined effects cooperatively inhibit the osteolytic cascade, forming a positive feedback mechanism that protects bone mass. The MDA-MB-231 apoptosis assay, the total apoptotic rate increased with escalating doses of Sabutoclax, which was primarily attributed to a rise in early apoptosis. At the animal study level, macroscopic analysis of our breast cancer-induced osteolysis model revealed a difference in volume of the experimental limbs between the high- and low-dose Sabutoclax treatment groups compared to the positive control group. Results from Micro-CT and immunohistochemical analyses consistently indicated that Sabutoclax inhibits bone resorption in vivo, thereby reducing breast cancer-induced osteolysis and protecting bone tis-

sue. In the present study, we investigated the effects of Sabutoclax on breast cancer cell lines using in vitro assays for proliferation, migration, invasion, and apoptosis, as well as an intratibial injection model in vivo. Several limitations of these experiments should be acknowledged. First, while our flow cytometry data (Annexin V/PI staining) demonstrated that Sabutoclax treatment increases the proportion of apoptotic MDA-MB-231 cells, we did not assess canonical apoptosis markers such as cleaved caspase-3 or cleaved PARP. Therefore, the precise apoptotic pathway activated by Sabutoclax in these cells and whether it proceeds through the expected mitochondrial pathway remains to be confirmed. Similarly, although we observed changes in BAX and BCL-2 mRNA expression, we did not examine BCL-2 family protein expression levels or verify target engagement in tumor cells. Future studies should include Western blot analysis of cleaved caspase-3, cleaved PARP, and BCL-2 family proteins to establish a more definitive mechanistic link. Second, we did not perform cell cycle analysis. As a result, we cannot distinguish whether the observed reduction in cell viability reflects true apoptotic cell death, cell cycle arrest, or a combination of both. We did not perform cell cycle analysis; therefore, we cannot distinguish whether the observed reduction in cell viability reflects true apoptotic cell death, cell cycle arrest, or a combination of both. This distinction is crucial for understanding whether Sabutoclax exerts cytostatic or cytotoxic effects, and represents an important direction for future investigation. This distinction is important for understanding the cytostatic versus cytotoxic effects of Sabutoclax. Third, and most importantly, our in vivo model, intratibial injection of MDA-MB-231 cells, represents a model of local tumor burden within the bone microenvironment, not a model of spontaneous bone metastasis. While this model allows assessment of tumor growth in the bone niche, it does not recapitulate the multi-step process of metastasis (intravasation, circulation, extravasation, and colonization of distant sites). Therefore, our findings should be interpreted as demonstrating that Sabutoclax inhibits the growth of breast cancer cells within the bone microenvironment, rather than it henhibiting the process of bone metastasis per se. To investigate effects on metastatic dissemination, future studies should employ more appropriate models, such as tail vein injection related to the experimental metastasis or orthotopic mammary fat pad injection with spontaneous metastasis to bone. In summary, our tumor cell data provide preliminary evidence that Sabutoclax exerts anti-tumor effects on breast cancer cells in vitro and in the bone microenvironment. However, the precise mechanisms of action and the distinction between effects on tumor cells versus effects on the bone microenvironment (e.g., via osteoclast inhibition) require further investigation using more specific molecular readouts and appropriate metastatic models.

Whether Sabutoclax inhibits the progression of the primary breast tumor or prevents bone metastasis *in vivo* requires further experimental investigation. We have established that Sabutoclax inhibits osteoclast differentiation by downregulating key factors such as NFATc1, c-Fos, and CTSK, and have confirmed its effects on the proliferation, migration, and apoptosis of cancer cells. However, as a pan-Bcl-2 inhibitor, its direct molecular targets and comprehensive impact on the entire signaling network and osteoclasts remain incompletely elucidated. Further research is needed in the future regarding the mechanism. The present study possesses several inherent limitations. The investigation is restricted to fundamental in vitro assays and small-animal models, without accompanying pharmacokinetic data, comprehensive systemic toxicity evaluation, or assessment of its impact on osteoblasts and other normal cell populations. Given that Sabutoclax functions as a pan-BCL-2 inhibitor, it carries the potential for off-target effects and hematological toxicity. Consequently, future studies should prioritize the investigation of its toxicity profile and safety considerations, which may ultimately inform therapeutic strategies for tumor bone metastasis.

Conclusion

In summary, this study demonstrates that Sabutoclax inhibits osteoclast differentiation, which is associated with the downregulation of NFATc1, c-Fos, and CTSK protein expression. Furthermore, by suppressing the function of breast cancer cells, Sabutoclax effectively prevents breast cancer-induced osteolysis. Therefore, this small-molecule compound warrants further evaluation in toxicity profile and safety

considerations preclinically to assess its therapeutic potential.

Disclosure of conflict of interest

None.

Address correspondence to: Jinmin Zhao and Jianwen Cheng, Department of Traumatic Orthopedics and Hand Surgery, The First Affiliated Hospital of Guangxi Medical University, Nanning 530021, Guangxi, China. E-mail: csgkswk@126.com (JMZ); 1730054162@qq.com (JWC)

References

[1] Zheng H, Bae Y, Kasimir-Bauer S, Tang R, Chen J, Ren G, Yuan M, Esposito M, Li W, Wei Y, Shen M, Zhang L, Tupitsyn N, Pantel K, King C, Sun J, Moriguchi J, Jun HT, Coxon A, Lee B and Kang Y. Therapeutic antibody targeting tumor- and osteoblastic niche-derived jagged1 sensitizes bone metastasis to chemotherapy. Cancer Cell 2017; 32: 731-747, e6.

[2] Furesi G, Rauner M and Hofbauer LC. Emerging players in prostate cancer-bone niche communication. Trends Cancer 2021; 7: 112-121.

[3] Sun J, Hu L, Bok S, Yallowitz AR, Cung M, McCormick J, Zheng LJ, Debnath S, Niu Y, Tan AY, Lalani S, Morse KW, Shinn D, Pajak A, Hammad M, Suhardi VJ, Li Z, Li N, Wang L, Zou W, Mittal V, Bostrom MPG, Xu R, Iyer S and Greenblatt MB. A vertebral skeletal stem cell lineage driving metastasis. Nature 2023; 621: 602-609.

[4] Nolan E, Kang Y and Malanchi I. Mechanisms of organ-specific metastasis of breast cancer. Cold Spring Harb Perspect Med 2023; 13: a041326.

[5] Jackett KN, Browne AT, Aber ER, Clements M and Kaplan RN. How the bone microenvironment shapes the pre-metastatic niche and metastasis. Nat Cancer 2024; 5: 1800-1814.

[6] Ye X, Huang X, Fu X, Zhang X, Lin R, Zhang W, Zhang J and Lu Y. Myeloid-like tumor hybrid cells in bone marrow promote progression of prostate cancer bone metastasis. J Hematol Oncol 2023; 16: 46.

[7] Whiteley AE, Ma D, Wang L, Yu SY, Yin C, Price TT, Simon BG, Xu KR, Marsh KA, Brockman ML, Prioleau TM, Zhou KI, Cui X, Fecci PE, Jeck WR, McCall CM, Neff JL and Sipkins DA. Breast cancer exploits neural signaling pathways for bone-to-meninges metastasis. Science 2024; 384: eadh5548.

[8] Zheng J, He W, Chen Y, Li L, Liang Q, Dai W, Li R, Chen F, Chen Z, Tan Y and Li X. Erianin serves as an NFATc1 inhibitor to prevent breast cancer-induced osteoclastogenesis and bone destruction. J Adv Res 2025; 69: 399-411.

[9] Bado IL, Zhang W, Hu J, Xu Z, Wang H, Sarkar P, Li L, Wan YW, Liu J, Wu W, Lo HC, Kim IS, Singh S, Janghorban M, Muscarella AM, Goldstein A, Singh P, Jeong HH, Liu C, Schiff R, Huang S, Ellis MJ, Gaber MW, Gugala Z, Liu Z and Zhang XH. The bone microenvironment increases phenotypic plasticity of ER(+) breast cancer cells. Dev Cell 2021; 56: 1100-1117, e9.

[10] McDonald MM, Khoo WH, Ng PY, Xiao Y, Zamerli J, Thatcher P, Kyaw W, Pathmanandavel K, Grootveld AK, Moran I, Butt D, Nguyen A, Corr A, Warren S, Biro M, Butterfield NC, Guilfoyle SE, Komla-Ebri D, Dack MRG, Dewhurst HF, Logan JG, Li Y, Mohanty ST, Byrne N, Terry RL, Simic MK, Chai R, Quinn JMW, Youlten SE, Pettitt JA, Abi-Hanna D, Jain R, Weninger W, Lundberg M, Sun S, Ebetino FH, Timpson P, Lee WM, Baldock PA, Rogers MJ, Brink R, Williams GR, Bassett JHD, Kemp JP, Pavlos NJ, Croucher PI and Phan TG. Osteoclasts recycle via osteomorphs during RANKL-stimulated bone resorption. Cell 2021; 184: 1330-1347, e13.

[11] Liang W, Feng R, Li X, Duan X, Feng S, Chen J, Li Y, Chen J, Liu Z, Wang X, Ruan G, Tang S, Ding C, Huang B, Zou Z and Chen T. A RANKL-UCHL1-sCD13 negative feedback loop limits osteoclastogenesis in subchondral bone to prevent osteoarthritis progression. Nat Commun 2024; 15: 8792.

[12] Yue Z, Niu X, Yuan Z, Qin Q, Jiang W, He L, Gao J, Ding Y, Liu Y, Xu Z, Li Z, Yang Z, Li R, Xue X, Gao Y, Yue F, Zhang XH, Hu G, Wang Y, Li Y, Chen G, Siwko S, Gartland A, Wang N, Xiao J, Liu M and Luo J. RSPO2 and RANKL signal through LGR4 to regulate osteoclastic premetastatic niche formation and bone metastasis. J Clin Invest 2022; 132: e144579.

[13] Liang QL, Xu HG, Yu L, Ding MR, Li YT, Qi GF, Zhang K, Wang L, Wang H and Cui X. Binding-induced fibrillogenesis peptide inhibits RANKL-mediated osteoclast activation against osteoporosis. Biomaterials 2023; 302: e122331.

[14] Fischer V and Haffner-Luntzer M. Interaction between bone and immune cells: implications for postmenopausal osteoporosis. Semin Cell Dev Biol 2022; 123: 14-21.

[15] Zhang M, Tang C, Li S, Jiang X, Li B, Chen Y, Zheng Q, Tang Y, Zhu X, Huang L, Yuan H, Wang J, Yin Y, Jin Y and Ma C. NSUN2-mediated m^5C modification of KDM6B mRNA enhances osteoclast differentiation and promotes breast cancer bone metastasis. Cancer Lett 2025; 631: 217939.

[16] Bird L. NFAT: platelet stickiness regulator. Nat Rev Immunol 2022; 22: 74-75.
[17] Latif MU, Schmidt GE, Mercan S, Rahman R, Gibhardt CS, Stejerean-Todoran I, Reutlinger K, Hessmann E, Singh SK, Moeed A, Rehman A, Butt UJ, Bohnenberger H, Stroebel P, Bremer SC, Neesse A, Bogeski I and Ellenrieder V. NFATc1 signaling drives chronic ER stress responses to promote NAFLD progression. Gut 2022; 71: 2561-2573.
[18] Hasselluhn MC, Schlösser D, Versemann L, Schmidt GE, Ulisse M, Oschwald J, Zhang Z, Hamdan F, Xiao H, Kopp W, Spitalieri J, Kellner C, Schneider C, Reutlinger K, Nagarajan S, Steuber B, Sastra SA, Palermo CF, Appelhans J, Bohnenberger H, Todorovic J, Kostyuchek I, Ströbel P, Bockelmann A, König A, Ammer-Herrmenau C, Schmidleitner L, Kaulfuß S, Wollnik B, Hahn SA, Neesse A, Singh SK, Bastians H, Reichert M, Sax U, Olive KP, Johnsen SA, Schneider G, Ellenrieder V and Hessmann E. An NFATc1/SMAD3/cJUN complex restricted to SMAD4-deficient pancreatic cancer guides rational therapies. Gastroenterology 2024; 166: 298-312, e14.
[19] Qiu Z, Li L, Huang Y, Shi K, Zhang L, Huang C, Liang J, Zeng Q, Wang J, He X, Qin L and Wang X. Puerarin specifically disrupts osteoclast activation via blocking integrin-β3 Pyk2/Src/Cbl signaling pathway. J Orthop Translat 2022; 33: 55-69.
[20] Jin L, Chen Y, Cheng D, He Z, Shi X, Du B, Xi X, Gao Y and Guo Y. YAP inhibits autophagy and promotes progression of colorectal cancer via upregulating Bcl-2 expression. Cell Death Dis 2021; 12: 457.
[21] Zhou X, Zhao J, Yan T, Ye D, Wang Y, Zhou B, Liu D, Wang X, Zheng W, Zheng B, Qian F, Li Y, Li D and Fang L. ANXA9 facilitates S100A4 and promotes breast cancer progression through modulating STAT3 pathway. Cell Death Dis 2024; 15: 260.
[22] D'Aguanno S, Brignone M, Scalera S, Chiacchiarini M, Di Martile M, Valentini E, De Nicola F, Ricci A, Pelle F, Botti C, Maugeri-Saccà M and Del Bufalo D. Bcl-2 dependent modulation of Hippo pathway in cancer cells. Cell Commun Signal 2024; 22: 277.
[23] Quinn BA, Dash R, Sarkar S, Azab B, Bhoopathi P, Das SK, Emdad L, Wei J, Pellecchia M, Sarkar D and Fisher PB. Pancreatic cancer combination therapy using a bh3 mimetic and a synthetic tetracycline. Cancer Res 2015; 75: 2305-2315.
[24] Goff DJ, Court Recart A, Sadarangani A, Chun HJ, Barrett CL, Krajewska M, Leu H, Low-Marchelli J, Ma W, Shih AY, Wei J, Zhai D, Geron I, Pu M, Bao L, Chuang R, Balaian L, Gotlib J, Minden M, Martinelli G, Rusert J, Dao KH, Shazand K, Wentworth P, Smith KM, Jamieson CA, Morris SR, Messer K, Goldstein LS, Hudson TJ, Marra M, Frazer KA, Pellecchia M, Reed JC and Jamieson CH. A Pan-BCL2 inhibitor renders bone-marrow-resident human leukemia stem cells sensitive to tyrosine kinase inhibition. Cell Stem Cell 2013; 12: 316-28.
[25] Arnold M, Morgan E, Rumgay H, Mafra A, Singh D, Laversanne M, Vignat J, Gralow JR, Cardoso F, Siesling S and Soerjomataram I. Current and future burden of breast cancer: global statistics for 2020 and 2040. Breast 2022; 66: 15-23.
[26] Zhu Q, Fu Y, Cui CP, Ding Y, Deng Z, Ning C, Hu F, Qiu C, Yu B, Zhou X, Yang G, Peng J, Zou W, Liu CH and Zhang L. OTUB1 promotes osteoblastic bone formation through stabilizing FGFR2. Signal Transduct Target Ther 2023; 8: 142.
[27] Bull EC, Singh A, Harden AM, Soanes K, Habash H, Toracchio L, Carrabotta M, Schreck C, Shah KM, Riestra PV, Chantoiseau M, Da Costa MEM, Moquin-Beaudry G, Pantziarka P, Essiet EA, Gerrand C, Gartland A, Bojmar L, Fahlgren A, Marchais A, Papakonstantinou E, Tomazou EM, Surdez D, Heymann D, Cidre-Aranaz F, Fromigue O, Sexton DW, Herold N, Grünewald TGP, Scotlandi K, Nathrath M and Green D. Targeting metastasis in paediatric bone sarcomas. Mol Cancer 2025; 24: 153.
[28] Satcher RL and Zhang XH. Evolving cancer-niche interactions and therapeutic targets during bone metastasis. Nat Rev Cancer 2022; 22: 85-101.
[29] Yunyun Z, Guihu W and An J. Explore the expression of mitochondria-related genes to construct prognostic risk model for ovarian cancer and validate it, so as to provide optimized treatment for ovarian cancer. Front Immunol 2024; 15: e1458264.
[30] Melo G, Silva CAB, Hague A, Parkinson EK and Rivero ERC. Anticancer effects of putative and validated BH3-mimetic drugs in head and neck squamous cell carcinomas: an overview of current knowledge. Oral Oncol 2022; 132: 105979.
[31] Kostel Bal S, Giuliani S, Block J, Repiscak P, Hafemeister C, Shahin T, Kasap N, Ransmayr B, Miao Y, van de Wetering C, Frohne A, Jimenez Heredia R, Schuster M, Zoghi S, Hertlein V, Thian M, Bykov A, Babayeva R, Bilgic Eltan S, Karakoc-Aydiner E, Shaw LE, Chowdhury I, Varjosalo M, Argüello RJ, Farlik M, Ozen A, Serfling E, Dupré L, Bock C, Halbritter F, Hannich JT, Castanon I, Kraakman MJ, Baris S and Boztug K. Biallelic NFATC1 mutations cause an inborn error of immunity with impaired CD8+ T-cell function and perturbed glycolysis. Blood 2023; 142: 827-845.

[32] Xie Q, Du X, Liang J, Shen Y, Ling Y, Huang Z, Ke Z, Li T, Song B, Wu T, Wang Y and Tao H. FABP4 inhibition suppresses bone resorption and protects against postmenopausal osteoporosis in ovariectomized mice. Nat Commun 2025; 16: 4437.

[33] Xue P, Zhang W, Shen M, Yang J, Chu J, Wang S, Wan M, Zheng J, Qiu Z and Cao X. Proton-activated chloride channel increases endplate porosity and pain in a mouse spine degeneration model. J Clin Invest 2024; 134: 168155.

[34] Xiu C, Luo H, Huang W, Fan S, Yuan C, Chen J, Xu C, Yao C, Hong D and Zhang L. Lobetyolin suppressed osteoclastogenesis and alleviated bone loss in ovariectomy-induced osteoporosis via hindering p50/p65 nuclear translocation and downstream NFATc1/c-fos expression. Drug Des Devel Ther 2025; 19: 4689-4715.